

Flexural ductility of prestressed concrete beams with unbonded tendons

F. T. K. Au[†], K. H. E. Chan[‡] and A. K. H. Kwan^{††}

Department of Civil Engineering, The University of Hong Kong, Hong Kong, China

J. S. Du^{‡‡}

School of Civil Engineering, Beijing Jiao Tong University, Beijing 100044, China

(Received May 6, 2008, Accepted September 14, 2009)

Abstract. Based on a numerical method to analyse the full-range behaviour of prestressed concrete beams with unbonded tendons, parametric studies are carried out to investigate the influence of 11 parameters on the curvature ductility of unbonded prestressed concrete (UPC) beams. It is found that, among various parameters studied, the depth to prestressing tendons, depth to non-prestressed tension steel, partial prestressing ratio, yield strength of non-prestressed tension steel and concrete compressive strength have substantial effects on the curvature ductility. Although the curvature ductility of UPC beams is affected by a large number of factors, rather simple equations can be formulated for reasonably accurate estimation of curvature ductility. Conversion factors are introduced to cope with the difference in partial safety factors, shapes of equivalent stress blocks and the equations to predict the ultimate tendon stress in BS8110, EC2 and ACI318. The same equations can also be used to provide conservative estimates of ductility of UPC beams with compression steel.

Keywords: curvature ductility; full-range behaviour; prestressed concrete; unbonded tendon.

1. Introduction

Unbonded prestressing has been gaining popularity in the construction of bridges and buildings. One reason is the potential corrosion risks with internal bonded tendons caused by incomplete penetration of grout. Another benefit of unbonded prestressing is the ease of tendon replacement which may be required during the life of the structure. With the increasing use of unbonded prestressed concrete (UPC) structures, there is a need for a closer examination of their design and analysis.

Investigations of UPC members over the past five decades have mainly focused on the tendon stress at ultimate. Recent work in this aspect has been extended to UPC members made of high-strength concrete (Ozkul *et al.* 2008) and those with fibre-reinforced polymer (FRP) tendons (Du and Au 2009). Comprehensive state-of-the-art reviews were reported by Naaman and Alkhairi

[†] Associate Professor, Corresponding author, E-mail: francis.au@hku.hk

[‡] Research Student, E-mail: enoch@hkusua.hku.hk

^{††} Professor, E-mail: khkwan@hku.hk

^{‡‡} Associate Professor, E-mail: dujsh97@mails.tsinghua.edu.cn

(1991), Allouche *et al.* (1998) and Au and Du (2004). Numerical modelling of UPC members has also been reported by various researchers, such as Harajli *et al.* (1999) and Du *et al.* (2008). The flexural ductility of UPC members has begun to gain more attention (Jo *et al.* 2004, Du *et al.* 2008). While the ultimate moment sets the upper limit of load carrying capacity of the structure, the flexural ductility is a measure of its ability to give sufficient warning before failure. Under extreme loading, such as blasting and earthquake, a ductile member forms plastic hinges which deform substantially beyond elasticity while maintaining sufficient flexural strength to resist the applied loads. The present philosophy of seismic design relies on energy absorption and dissipation by the post-elastic deformation for survival in major earthquakes. A structure with higher ductility will have a lower chance of collapse. There are, however, no detailing rules to ensure a minimum flexural ductility for UPC beams in British code BS8110 (British Standards Institution 1997) and European code EC2 (European Committee for Standardisation 2004). In American code ACI318 (ACI Committee 318 2005), both UPC and reinforced concrete (RC) beams have the same provisions pertaining to flexural ductility, although it is questionable if these limits could ensure the same degree of safety in both types with their disparity in design and detailing. To suppress tensile stresses, UPC beams are subjected to axial compressive forces induced by high-tensile steel wires or strands. Unlike ordinary steel reinforcement, these tendons do not possess a distinct yield point. Furthermore, the tendon profiles may be straight, harped or even parabolic. External tendons may even be placed below the soffit. It should also be noted that UPC beams are usually adopted in comparatively long spans as compared to RC beams, and hence UPC beam sections are usually deeper than RC beam sections. Most codes, including BS8110, EC2 and ACI318, require surface or skin reinforcement to be placed near the vertical faces of tension zone to control cracking in the web. The surface or skin reinforcement reduces the depth to the centroid of non-prestressed steel relative to the total height. As a result, another set of detailing rules is required to cater for UPC members.

To evaluate the flexural ductility, it is necessary to obtain the full-range behaviour which covers not only the service stage up to the peak carrying capacity, but also extends well into the post-peak range. Concrete beams with bonded and unbonded tendons behave differently especially when overloaded although they behave in a similar manner at the working stage. The behaviour of prestressed concrete (PC) beams with bonded tendons is characterised by that at individual sections, as there is bonding between the tendons and the surrounding concrete. However this is not the case for PC beams with unbonded tendons because the tendons and the surrounding concrete generally slip with respect to each other. The stress increase in tendons due to external loading subsequent to prestressing depends on the deformation of the whole member, and it cannot be determined from the analysis of the cross sections alone as in the case of bonded tendons. A non-linear analysis of the entire member is therefore necessary.

A theoretical method for complete moment-curvature analysis of UPC beams (Du *et al.* 2008) has been developed recently. Apart from tendon slip, the model can also simulate the post-peak behaviour of the member taking into account the strain reversal in non-prestressed steel and concrete at the descending branches of the stress-strain curves. It is necessary to consider the stress-path dependence because as the plastic hinges formed in a beam enter the post-peak stage, the other sections will be unloaded. Using the method, the influence of various factors on the flexural ductility is investigated. These factors include the amount of steel reinforcement, span-depth ratio, type of loading, tendon profile, partial prestressing ratio *PPR*, effective prestressing ratio, yield strength of non-prestressed steel, concrete strength, depths to prestressed and non-prestressed steel

as well as size effect. With the critical parameters identified, simple rules can then be developed for convenient application to engineering design or adoption in codes of practice. In the light of findings from the parametric studies, practical design rules are proposed.

2. Moment-curvature analysis

The assumptions made in the numerical model include (a) plane sections remain plane after bending; (b) the constitutive relations for prestressing tendons, non-prestressed steel and concrete are known; (c) the friction between the concrete and prestressing tendons is neglected; and (d) the member has adequate shear strength.

2.1. Material properties

The stress-strain relationship for concrete in compression as proposed by Attard and Setunge (1996) has been shown to be applicable to a broad range of concrete strength from 20 to 130 MPa, and is used in the study. The parameters to establish the equation include the modulus of elasticity of concrete E_c , *in situ* concrete strength f_{co} , strain at peak stress ε_{co} , and the stress f_{ci} and strain ε_{ci} at the inflection point on the descending branch of the stress-strain curve. The *in situ* concrete strength f_{co} can be obtained from the cylinder strength or cube strength by suitable conversion factors. The concrete stress σ_c is related to the concrete strain ε_c by

$$\frac{\sigma_c}{f_{co}} = \frac{A(\varepsilon_c/\varepsilon_{co}) + B(\varepsilon_c/\varepsilon_{co})^2}{1 + (A-2)(\varepsilon_c/\varepsilon_{co}) + (B+1)(\varepsilon_c/\varepsilon_{co})^2} \quad (1)$$

in terms of parameters A and B , which depend on the concrete grade. The stress-strain relationship for concrete in tension is assumed to be linear with a slope equal to the elastic modulus in compression at zero stress. The tensile strength of concrete is taken as $0.1f_{co}$. The contribution of concrete in tension after cracking is neglected. The model of Bahn and Hsu (1998) for the unloading stress-strain relationship of concrete is adopted, namely

$$\frac{\sigma_{unlo}}{f_{co}} = 0.95 \frac{\sigma_c}{f_{co}} \left(\frac{\varepsilon_{unlo}/\varepsilon_{co} - \varepsilon_{cp}/\varepsilon_{co}}{\varepsilon_c/\varepsilon_{co} - \varepsilon_{cp}/\varepsilon_{co}} \right)^{1 + \sqrt{\varepsilon_{cp}/\varepsilon_{co}}} \quad (2a)$$

$$\frac{\varepsilon_{cp}}{\varepsilon_{co}} = 0.30 \left(\frac{\varepsilon_c}{\varepsilon_{co}} \right)^2 \quad (2b)$$

where σ_{unlo} and ε_{unlo} are respectively the stress and strain in concrete on unloading; σ_c and ε_c are respectively the stress and strain in concrete in Eq. (2a); ε_{cp} is the residual plastic strain in concrete corresponding to unloading from point $(\varepsilon_c, \sigma_c)$; and ε_{co} is concrete strain at peak stress f_{co} . Fig. 1 shows the loading and unloading curves adopted in the study.

The non-prestressed steel is assumed to be perfectly elasto-plastic as shown in Fig. 2. To cater for strain reversal, the stress-path dependence of the stress-strain relation is taken into account by assuming that the unloading path follows the initial elastic slope. The stress-strain formula for prestressing steel proposed by Menegotto and Pinto (1973) was shown by Naaman (1985) to be realistic, and it is adopted here. The stress σ_{ps} is related to the strain ε_p by

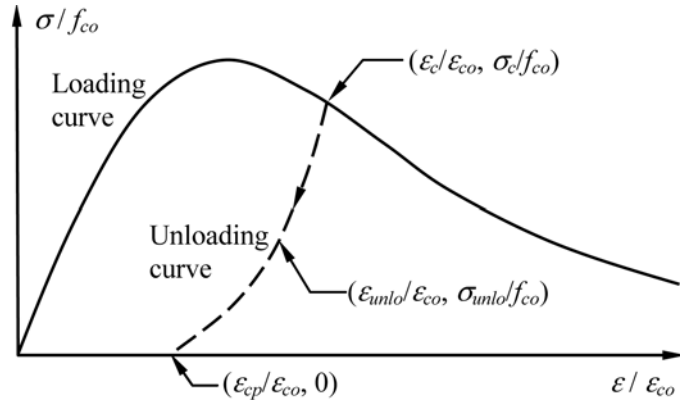


Fig. 1 Stress-strain curve for concrete

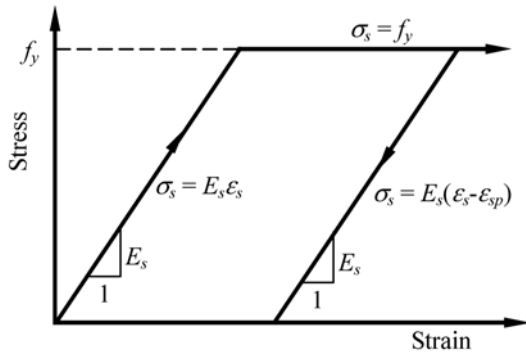


Fig. 2 Stress-strain relationship of non-prestressed steel allowing for stress-path dependence

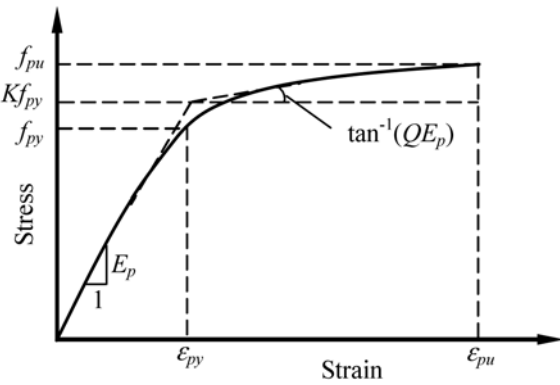


Fig. 3 Stress-strain relationship of prestressing tendons

$$\sigma_{ps} = E_p \varepsilon_p \left\{ Q + \frac{1-Q}{[1 + (E_p \varepsilon_p / K f_{py})^N]^{1/N}} \right\} \tag{3a}$$

$$Q = \frac{f_{pu} - K f_{py}}{E_p \varepsilon_{pu} - K f_{py}} \tag{3b}$$

as shown in Fig. 3 where E_p is the modulus of elasticity of prestressing steel; f_{py} is the yield stress of prestressing steel; f_{pu} and ε_{pu} are the ultimate stress and strain of prestressing steel, respectively; and the empirical parameters N , K and Q are respectively 7.344, 1.0618 and 0.01174 for 7-wire strands of ASTM Grade 270 with ultimate tensile strength of $f_{pu}=1863$ MPa.

2.2. Numerical procedures

It is assumed that a symmetrically loaded beam also fails symmetrically with a plastic hinge formed at mid-span. For the analysis, half of the beam is subdivided into m elements ($k = 1, 2, \dots, m$) as shown in Fig. 4. For convenience, the first element ($k = 1$) at the centre of the beam is taken as the control element where the concrete strain at the top fibre is increased by increments to

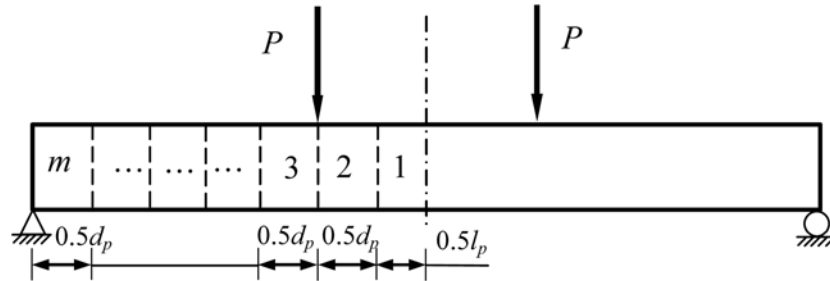


Fig. 4 Arrangement of elements along the beam for analysis

simulate the applied loading or imposed displacement. The length of the control element is taken as half of the plastic hinge length l_p , while the length of the other elements is about $0.5d_p$ where d_p is the depth to centroid of tendon. As recommended by Harajli (1990), Corley's expression for the plastic hinge length l_p as modified by Mattock (1967) is adopted.

For each value of concrete strain at the top fibre of the control element, a three-level iteration procedure is carried out to satisfy the following criteria: (a) equilibrium of forces across the depth of all elements; (b) equilibrium between the externally applied load and the internal moment resistance at each element; and (c) compatibility of the average strain and average elongation between the end anchorages of the unbonded tendons. The concrete strain at the top fibre of the control element is increased monotonically until the moment at which the control element has experienced its peak moment and dropped to 85% of the peak value.

2.3. Verification of numerical results

The numerical results are verified by comparison of the load-deflection curves with some experimental results. When a UPC beam is loaded, the load-deflection curves normally exhibits four stages, namely (a) elastic, (b) cracked-elastic, (c) pre-peak plastic and (d) post-peak stage. In some cases the last two stages are considered together as one for convenience. The transition from the first to the second stages is caused by cracking, while the transition from the second to the third stage is caused by yielding of the non-prestressed steel. In the work of Du and Tao (1985) on simply supported partially prestressed concrete (PPC) beams with unbonded and bonded tendons, all the test beams were 160 mm×280 mm and were tested with third-point loading over a 4200 mm span. The ratio of the span L to the effective depth d_p at mid-span, or span-depth ratio unless otherwise stated, was 19.1. The UPC beams were divided into three categories and each beam was designed for the non-prestressed steel to carry about 30%, 50% and 70% of the total ultimate load. The reinforcement was characterized by the combined reinforcement index (CRI) q_0 at mid-span defined as

$$q_0 = \frac{A_p f_{pe} + A_s f_y}{b d_p f'_c} \quad (4)$$

where f_{pe} is the effective stress in prestressed steel; f_y is the yield strength of non-prestressed tension steel; f'_c is the cylinder strength of concrete; A_p is the cross-sectional area of prestressing steel; A_s is the cross-sectional areas of non-prestressed tension steel; b is the width of compression face of the beam; d_p is the distance from extreme compression fibre to centroid of prestressing steel.

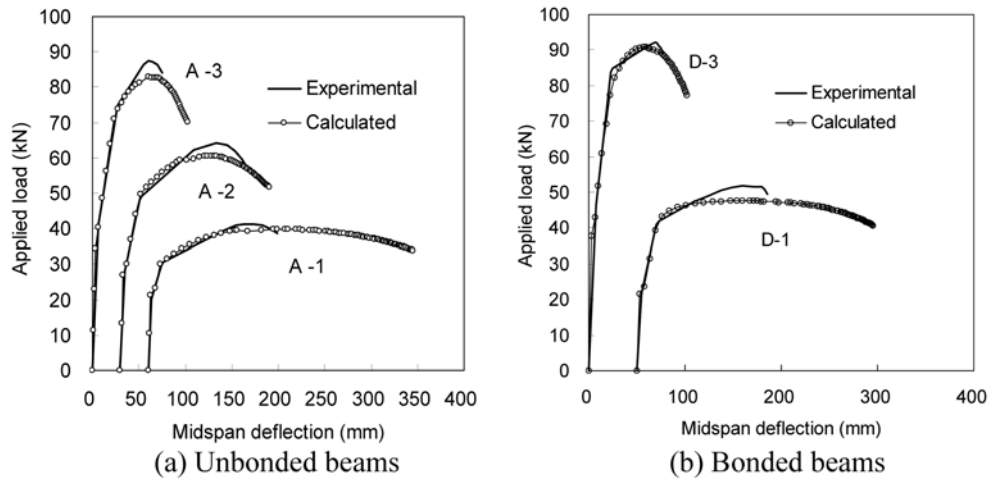


Fig. 5 Comparison of numerical results with experimental results of Du and Tao (1985)

The 26 PPC beams were divided into four groups, namely Groups A, B, C and D, which were unbonded except for those in Group D. The beams in Groups A, B and C were classified according to the CRI q_0 , namely low ($q_0 < 0.15$), medium ($0.15 < q_0 < 0.25$) and high ($q_0 > 0.25$). The 9 beams in Group A were further classified into three categories, each containing three beams corresponding to the three different levels of q_0 as stated above. Groups A and B were similar in that each beam in Group B was identical to one in Group A except that the strengths of the prestressing steel and concrete in the former were higher. Group C consisted of 4 beams which were identical to Beams A-1, A-3, A-7 and A-9, except that cold stretched bars of higher strength were used instead of ordinary non-prestressed steel. The 4 beams in Group D were largely duplicates of their counterparts in Group A except that those in Group D were bonded. Beam D-0 was an RC beam. The load-deflection curves for beams A-1, A-2 and A-3 in Group A and Beams D-1 and D-3 in Group D are plotted in Figs. 5(a) and 5(b), respectively. Good agreement can be seen between the numerical and experimental results.

3. Curvature ductility factor

The flexural ductility of a structural member is usually expressed in terms of a dimensionless ductility factor, which is the ratio of a kind of deformation at failure to that at yield. The curvature ductility factor μ_ϕ used here is defined in terms of the ultimate curvature ϕ_u and the curvature at first yield ϕ_y , as

$$\mu_\phi = \frac{\phi_u}{\phi_y} \quad (5)$$

The ultimate curvature ϕ_u is taken as the curvature of the section when the resisting moment has dropped to 85% of the peak resisting moment after reaching the peak, while the yield curvature ϕ_y , corresponds to that at the commencement of yielding. This definition as suggested by Park and Paulay (1975) gives a more reliable indication of how well a structure copes with overloading.

4. Factors affecting flexural ductility

The tendon stress in a UPC beam depends on deformation of the entire structure which is a function of various factors, such as the amount of steel reinforcement, span-depth ratio, type of loading, tendon profile, partial prestressing ratio *PPR*, effective prestressing ratio, yield strength of non-prestressed steel, concrete strength, depths to prestressed and non-prestressed steel as well as sectional dimensions. To develop simple design rules, the first step is to identify the factors which have more significant effect on curvature ductility.

In UPC beams, bonded non-prestressed steel is usually provided together with unbonded prestressed steel to assure post-cracking ductility so that a brittle failure will not develop upon first cracking. The total amount of flexural reinforcement in such a partial prestressing system is characterized by the reinforcement index ω defined as

$$\omega = \frac{A_p f_{ps} + A_s f_s - A'_s f'_s}{b d_{cf} f_{co}} \quad (6)$$

where A_p is the cross sectional area of prestressing tendon, A_s and A'_s are the cross sectional areas of the bottom and top non-prestressed steel respectively, b is the width of the section, d_{cf} is the depth to centroid of tensile force in reinforcement, f_{ps} is the stress in prestressing steel at peak load, f_s and f'_s are the stresses of the bottom and top non-prestressed steel at ultimate respectively, and f_{co} is the *in situ* concrete compressive strength. From a numerical study of bonded PC beams, Naaman *et al.* (1986) found that reinforcement index ω is an excellent independent variable for describing ductility since it is proportional to x/d_{cf} , where x is the distance from extreme compression fibre to neutral axis. An experimental study of UPC beams (Au *et al.* 2008) also demonstrates the same trend the lower the reinforcement index ω is, the higher is the beam ductility. The current study aims to identify if there are other parameters which should not be neglected in predicting the ductility of UPC beams. If the curvature ductility factors of UPC beams with similar reinforcement index ω are sensitive to the change of a certain parameter, then the parameter should be considered essential. To study the influence of the parameters, each parameter is varied in turn while the others are kept constant. However, in order to maintain the same reinforcement index and partial prestressing ratio, the amount of prestressed and non-prestressed steel may need to be adjusted by trial and error. In the parametric studies, ASTM grade 270 7-wire strands with ultimate tensile strength of $f_{pu} = 1863$ MPa are used and the following properties are adopted unless otherwise specified:

- (a) Rectangular section with width $b = 500$ mm, overall depth $h = 1000$ mm and depth to tendon $d_p = 0.85h$
- (b) Span-depth ratio $L / d_p = 20$
- (c) Loading type: point load at mid-span
- (d) Tendon profile: unbonded straight tendon
- (e) Partial prestressing ratio $PPR = 0.5$
- (f) Effective prestressing ratio = 50%
- (g) Non-prestressed steel: depth $d_s = 0.94h$ and yield strength $f_y = 460$ MPa
- (h) *In situ* concrete compressive strength $f_{co} = 50$ MPa

4.1. Span-depth ratios

UPC members with a wide range of ratios of span to depth to tendon are studied to examine their

effect. While maintaining the depth to tendon as $d_p = 0.85h$ and the depth to non-prestressed steel as $d_s = 0.94h$, span-depth ratios of 5, 10, 20, 30, 40 and 50 are achieved by varying the span length. The curvature ductility factor remains virtually the same within this range of span-depth ratio if reinforcement index ω , PPR and other parameters are held constant. For reinforcement indices ω of 0.1, 0.2 and 0.3, the corresponding average curvature ductility factors are 12.2, 4.55 and 2.46 respectively with the difference not exceeding 1.2% of the respective average values.

4.2. Loading types

The effect of three different loading types, namely central point load, third-point loading and uniform loading, is investigated. When the other parameters are kept constant, at a given reinforcement index ω , the curvature ductility factor is not significantly influenced by the loading type. The average curvature ductility factors for beams with reinforcement indices ω of 0.1, 0.2 and 0.3 are 12.3, 4.56 and 2.47 respectively. For a constant reinforcement index ω , the difference is not significant, with the difference not exceeding 1.2% of the respective average values.

4.3. Tendon profiles

In simply supported beams having harped or parabolic tendons, the tendon ends are usually located at the section centroid to minimize the bending moments induced there. The tendon profile can be defined by its shape and the depth to tendon at mid-span d_p . The effect of tendon depth at mid-span d_p is studied by varying it from $0.5h$ to $1.1h$, including the case of tendons located below the soffit to increase the moment arm. A harped tendon profile with the deviators located at the third points is studied. The results in Fig. 6 show that ductility decreases with increasing tendon depth at mid-span. Members with reinforcement indices ω of 0.1, 0.2 and 0.3 all follow the same trend.

The effect of the shape of tendon profile is also investigated for members with the same tendon depths at mid-span. Three different tendon profiles are adopted, namely straight, harped and parabolic profiles. For the harped profile, the shape can also be varied by changing the positions of deviators. It is found that variation in tendon profile has no significant effect on flexural ductility.

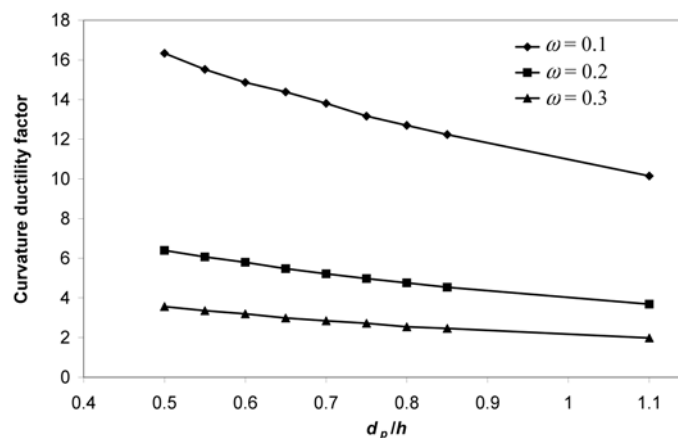


Fig. 6 Effect of depth to prestressing tendon d_p on ductility of UPC members

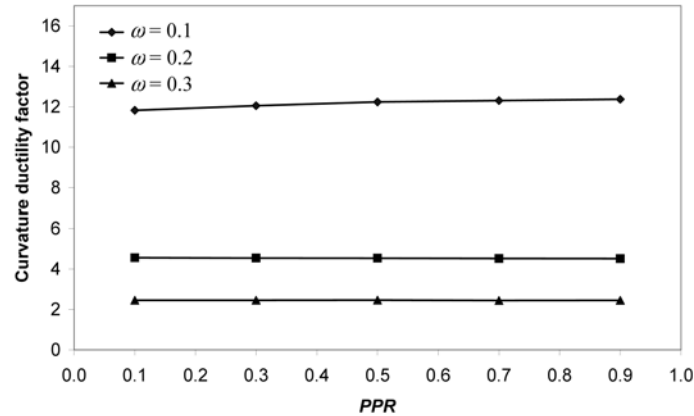


Fig. 7 Effect of PPR on ductility of UPC members

The variation in curvature ductility from the respective average value is less than 0.8% among the tendon shapes considered, including straight, parabolic and harped with a single deviator at mid-span or a pair of deviators at $0.167L$ or $0.333L$ from the mid-span, where L is the span length. The average curvature ductility factors for beams with reinforcement indices ω of 0.1, 0.2 and 0.3 are 12.2, 4.54 and 2.46 respectively.

4.4. Partial prestressing ratio PPR

The extent of prestressing is described by the partial prestressing ratio PPR defined as

$$PPR = \frac{A_p f_{ps}}{A_p f_{ps} + A_s f_s} \quad (7)$$

In the study, PPR is varied from 0.1 to 0.9 in order to assess its influence. Fig. 7 shows the variation of curvature ductility factor with PPR at different values of reinforcement index ω . For reinforcement index ω of 0.1, a mildly increasing trend in ductility factor can be observed as PPR increases, accounting for 2.8% of the average value. However, for reinforcement indices ω of 0.2 and 0.3, the variation in curvature ductility is minimal, being less than 0.6% of the respective average values.

4.5. Effective prestressing ratio

To investigate the effect of effective prestress f_{pe} , the strands are prestressed to 30%, 50% or 70% of the ultimate tensile strength. The variation of curvature ductility factor with the effective prestressing ratio f_{pe}/f_{pu} is presented in Fig. 8. It shows that the curvature ductility factor decreases slightly as the effective prestressing ratio increases for a given reinforcement index ω . For an increase of effective prestressing ratio from 30% to 70%, the reductions in curvature ductility factor are 4.1%, 2.6% and 1.7% for ω of 0.1, 0.2 and 0.3 respectively, which are not significant. Therefore the flexural ductility is more or less the same for various combinations of effective prestress f_{pe} and tendon area that give the same initial tendon force. This important finding gives flexibility in design.

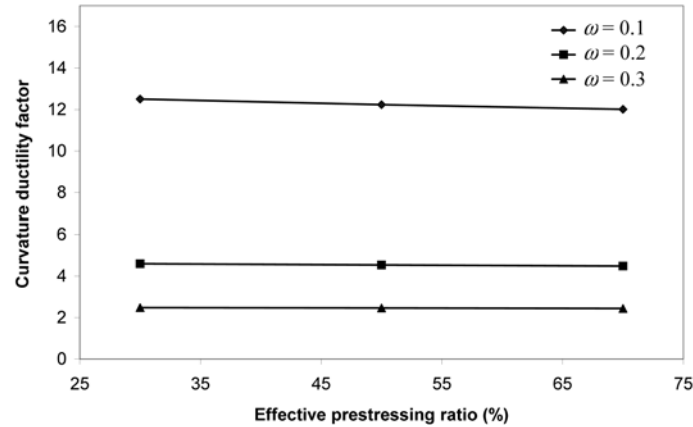


Fig. 8 Effect of effective prestressing ratio on ductility of UPC members

4.6. Non-prestressed steel

The depth to non-prestressed tension steel d_s is varied from $0.7h$ to $0.94h$ to investigate its effect. Some influence on flexural ductility is observed as shown in Fig. 9. For beams having the same reinforcement index ω , the curvature ductility factor increases with increasing depth to non-prestressed tension steel. Three cases of yield strength are investigated, namely $f_y = 250, 460$ and 600 MPa. The results in Fig. 10 show that, at a given reinforcement index ω with the other parameters held constant, an increase in yield strength leads to a significant decrease of curvature ductility factor.

4.7. Concrete compressive strength

To investigate the influence of *in situ* concrete compressive strength, four cases are studied, namely $f_{co} = 30, 50, 70$ and 90 MPa. The results in Fig. 11 show that when the reinforcement index

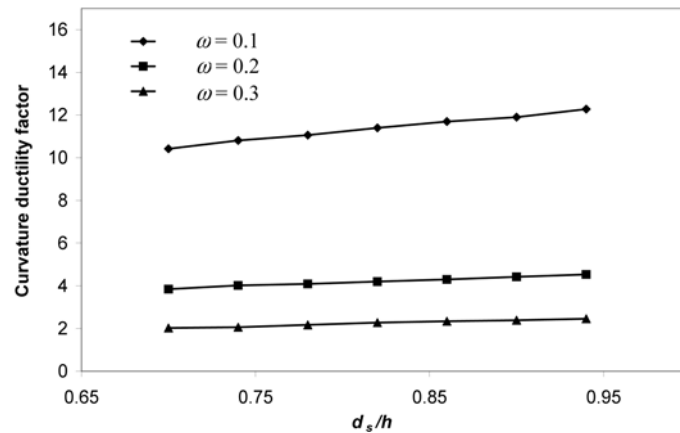


Fig. 9 Effect of depth to non-prestressed tension steel on ductility of UPC members

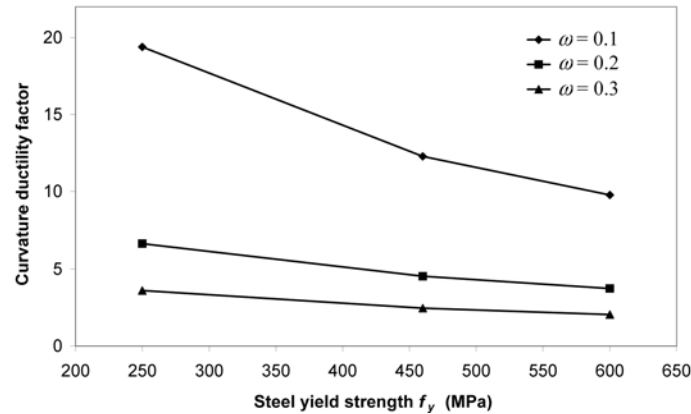
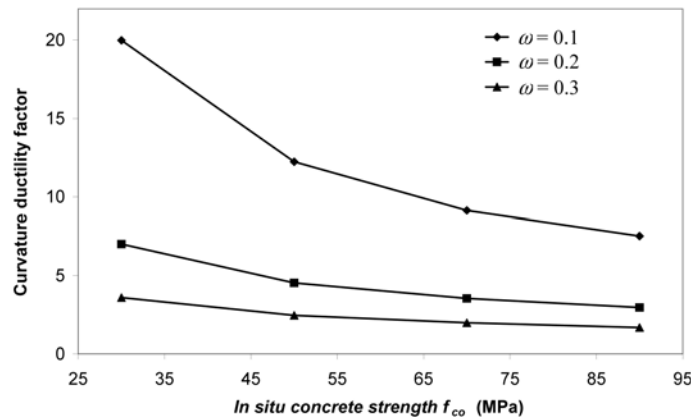


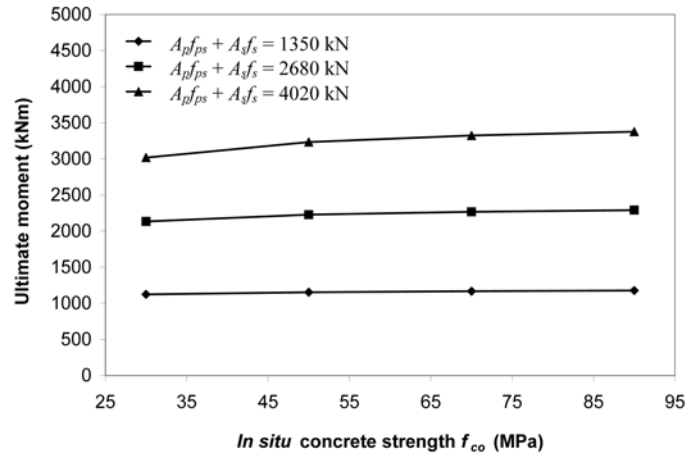
Fig. 10 Effect of steel yield strength on ductility of UPC members

Fig. 11 Effect of *in situ* concrete strength on ductility of UPC members

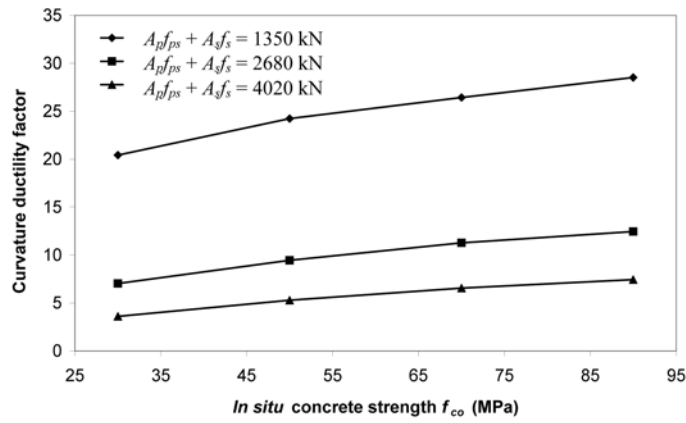
ω is kept constant, the curvature ductility factor drops substantially while the concrete compressive strength f_{co} increases, indicating that f_{co} is a key parameter affecting curvature ductility. As expected, for the same amount of prestressing tendons and non-prestressed steel, the ultimate moment capacity increases mildly with increasing concrete strength (Fig. 12(a)). On the other hand, although concrete with higher compressive strength is more brittle, it does not necessarily mean that UPC beams constructed with it are less ductile than those made of normal strength concrete. In fact, curvature ductility increases with concrete strength, given that the amount of prestressed and non-prestressed steel does not change. In Fig. 12(b), each curve represents the same tensile force at ultimate, i.e. $(A_p f_{ps} + A_s f_s)$, while PPR is taken as 0.5. It can be observed that curvature ductility factor increases with concrete strength. The increase in curvature ductility due to higher concrete strength provides margin for more reinforcement if a larger moment capacity is required.

4.8. Size effect

To investigate if the above findings are applicable to sections of different dimensions, two different cases are investigated: (a) the values of h , d_p , d_s , ω and PPR are kept fixed, while the



(a)



(b)

Fig. 12 Effect of *in situ* concrete strength on (a) ultimate moment and (b) curvature ductility of UPC members with various values of total tensile force at ultimate

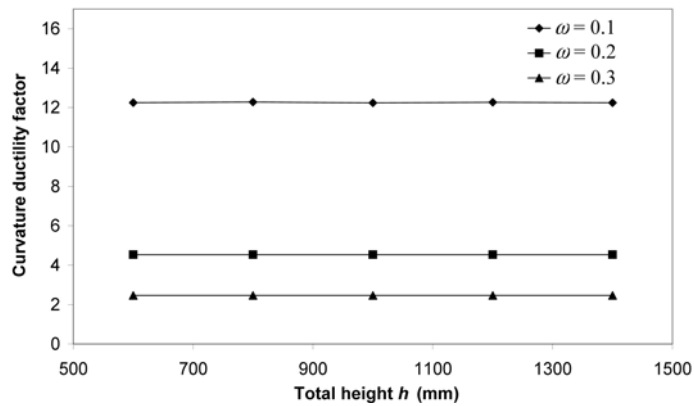


Fig. 13 Effect of total height h on ductility of UPC members

width b varies from 350 mm to 800 mm; and (b) the values of b , d_p/h , d_s/h , ω and PPR are kept fixed, while the total height h varies from 600 mm to 1400 mm. It is not surprising that the section width b has no effect on flexural ductility in the first case. The curvature ductility factors are 12.3, 4.54 and 2.46 for reinforcement indices ω of 0.1, 0.2 and 0.3 respectively, regardless of the section width b . The second case shows that the curvature ductility factor remains constant when the reinforcement index ω is kept unchanged (Fig. 13). The above implies that the findings presented here are not affected by the cross section size.

4.9. Discussions

The effects of various parameters on curvature ductility of UPC beams are reviewed. While keeping the reinforcement index ω unchanged, the curvature ductility factor varies by less than 1.2% of the average ductility factor for changes in span-depth ratio, load type, tendon shape or cross-section dimensions within the range studied. Considering the inherent uncertainties in material properties and variation in workmanship during construction, it can be concluded that the above group of parameters (i.e. Group 1) have minor influence on curvature ductility in members with equal reinforcement index ω . The other group of parameters (i.e. Group 2), which include the depth to non-prestressed tension steel d_s , depth to prestressing tendon at mid-span d_p , partial prestressing ratio PPR , yield strength of non-prestressed steel f_y and *in situ* concrete compressive strength f_{co} , have more substantial effect on curvature ductility, and hence they cannot be neglected in estimating the curvature ductility factors of UPC beams.

5. Estimation of curvature ductility of UPC beams

The next stage of parametric study is to investigate the simultaneous effect of two or more of the parameters in Group 2. The following ranges of parameters are considered: reinforcement index $\omega = 0.1-0.6$; partial prestressing ratio $PPR = 0.1-0.9$; depth to non-prestressed tension steel $d_s = 0.75h-0.95h$; depth to prestressing tendon at mid-span $d_p = 0.6h-1.1h$; yield strength of non-prestressed

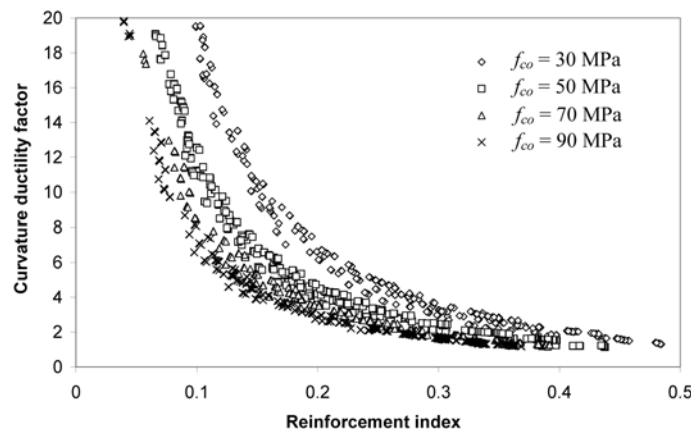


Fig. 14 Summary of parametric studies: variation of curvature ductility factor μ with respect to reinforcement index ω

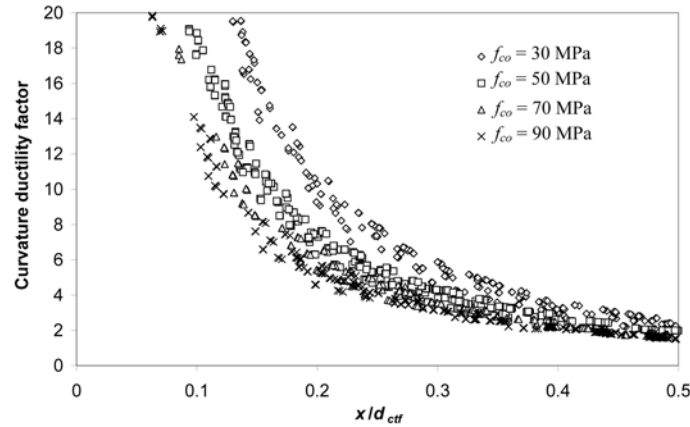


Fig. 15 Summary of parametric studies: variation of curvature ductility factor μ with respect to x/d_{cif}

steel $f_y = 250, 460$ or 600 MPa and *in situ* concrete compressive strength $f_{co} = 30, 50, 70$ or 90 MPa. Although design standards BS8110 and ACI318 permit a maximum prestressing ratio of 70%, taking an average loss of prestress of 20% (Lin and Burns 1981), a typical effective prestressing ratio of 50% is adopted. The most conservative scenarios for parameters in Group 1 are assumed. This ensures that the estimated curvature ductility factor is slightly on the safe side, as the deviation does not exceed 1.2% of the average value for any changes of parameters in Group 1 within the range studied.

Figs. 14 and 15 present some typical results from the parametric studies. In general, for members having the same depth to prestressing tendon d_p , concrete compressive strength f_{co} and steel yield strength f_y , the curvature ductility factor tends to cluster within a narrow band for the same reinforcement index ω or x/d_{cif} ratio. As expected, the curvature ductility μ_ϕ decreases with increasing reinforcement index ω or x/d_{cif} ratio. A lower bound equation can therefore be fitted to each band to provide a conservative estimate of curvature ductility factor for the design of UPC beams, namely

$$\mu_\phi = \frac{1}{a_1\omega + a_2\omega^2 + a_3\omega^3 + a_4\omega^4} \quad (8)$$

The coefficients a_1, a_2, a_3 and a_4 for various cases are shown in Table 1. Since BS8110 and EC2 impose limits on x/d to ensure a minimum level of curvature ductility where d is the effective depth, one may similarly express the lower bound equations in terms of the ratio x/d_{cif} as

$$\mu_\phi = \frac{1}{b_1(x/d_{cif}) + b_2(x/d_{cif})^2 + b_3(x/d_{cif})^3 + b_4(x/d_{cif})^4} \quad (9)$$

The coefficients b_1, b_2, b_3 and b_4 for various cases are also shown in Table 1. Unlike BS8110 and EC2, the 2005 version of ACI318 imposes limits on the net tensile strain of the extreme tension steel ε_t to classify sections as compression-controlled, tension-controlled or those in between. Since the code has prescribed the maximum usable strain at extreme concrete compression fibre to be 0.003, the parameters x/d_{cif} and ε_t can be related by the plane-section assumption. If the prestressed and non-prestressed reinforcement are placed at the same depth from the extreme compressive fibre,

Table 1 Coefficients for Eqs. (8) and (9) and x/d_{cf} conversion factors for UPC beams

Steel yield strength f_y	d_p/h	<i>In situ</i> concrete strength f_{co}	Coefficients for equations (12) and (13)								x/d conversion factors for		
			a_1	a_2	a_3	a_4	b_1	b_2	b_3	b_4	BS 8110	EC 2	ACI 318
250	0.60	30	0.0	4.0	-10.1	12.3	-0.1	3.2	-6.7	5.8	0.78	0.84	1.00
		50	0.2	3.7	-8.3	11.7	0.1	2.6	-5.2	4.8	0.83	0.89	0.87
		70	0.4	3.3	-5.3	8.3	0.2	1.8	-2.7	2.5	0.89	0.78	0.92
		90	0.5	3.0	-0.9	0.3	0.3	1.6	-1.7	1.8	0.93	0.67	0.96
	0.85	30	0.2	1.8	-1.1	2.4	-0.2	4.6	-10.6	9.9	0.80	0.89	1.04
		50	0.4	1.5	1.6	-0.5	-0.1	5.7	-14.0	13.2	0.87	0.93	0.89
		70	0.3	5.8	-17.7	28.9	0.3	2.2	-3.1	3.1	0.92	0.81	0.94
		90	0.5	5.4	-16.3	32.6	0.3	2.5	-4.2	4.7	0.97	0.69	0.97
	1.1	30	-0.3	11.8	-43.1	64.1	-0.4	9.4	-28.2	33.3	0.83	0.93	1.06
		50	0.0	14.0	-58.9	98.5	0.0	6.7	-17.7	20.7	0.90	0.96	0.90
		70	0.4	11.0	-44.4	84.8	0.3	4.2	-8.3	10.3	0.95	0.83	0.95
		90	0.7	8.6	-34.1	82.2	0.5	4.1	-8.9	12.8	1.00	0.70	0.98
460	0.60	30	0.0	7.1	-20.8	27.8	-0.2	5.8	-15.1	15.3	0.78	0.84	1.02
		50	0.3	7.6	-24.1	35.7	0.0	5.9	-15.5	15.6	0.84	0.90	0.87
		70	0.6	5.9	-14.8	23.6	0.4	2.8	-5.2	5.6	0.90	0.79	0.92
		90	0.9	5.3	-9.3	14.3	0.4	3.3	-6.2	6.1	0.96	0.67	0.96
	0.85	30	0.2	3.3	-2.6	2.9	0.1	2.8	-4.8	6.1	0.81	0.90	1.05
		50	0.4	6.6	-16.7	23.4	0.0	7.4	-21.2	24.0	0.88	0.94	0.90
		70	0.5	9.1	-25.5	32.6	0.4	4.2	-9.5	11.1	0.94	0.81	0.93
		90	0.5	12.2	-38.6	50.8	0.6	2.9	-3.7	3.5	0.99	0.69	0.97
	1.1	30	0.5	4.5	-8.1	17.7	-0.3	10.6	-34.2	46.9	0.84	0.93	1.07
		50	1.1	2.8	-2.0	11.2	0.4	6.1	-15.2	21.8	0.91	0.96	0.90
		70	1.8	-3.4	26.3	-16.2	0.7	4.7	-8.4	11.7	0.96	0.84	0.96
		90	2.0	0.2	9.5	6.6	0.7	6.4	-15.3	20.0	1.01	0.70	0.99
600	0.60	30	0.2	5.6	-13.3	19.8	0.1	3.9	-9.1	10.7	0.78	0.85	1.02
		50	0.4	10.0	-35.4	55.9	0.3	4.5	-10.7	11.8	0.84	0.90	0.88
		70	0.7	9.0	-32.2	57.8	0.4	5.3	-15.3	18.3	0.90	0.80	0.94
		90	1.3	4.4	-13.6	41.5	0.8	1.9	-1.2	1.7	0.96	0.68	0.98
	0.85	30	0.2	7.2	-23.4	38.7	-0.7	14.1	-45.5	53.1	0.81	0.91	1.07
		50	0.5	9.3	-31.5	54.0	0.1	9.1	-28.1	34.2	0.88	0.95	0.92
		70	1.1	6.3	-25.2	57.5	0.3	8.9	-30.0	38.8	0.95	0.83	0.95
		90	1.3	6.6	-23.1	51.4	0.9	2.6	-2.0	2.2	0.99	0.70	1.00
	1.1	30	1.3	-5.2	31.8	-24.2	-0.2	12.1	-43.9	67.7	0.84	0.95	1.10
		50	0.9	5.4	5.5	-4.0	-0.1	17.4	-71.0	110.8	0.91	0.99	0.95
		70	1.4	6.5	-9.1	26.5	0.6	10.8	-39.0	61.7	0.97	0.85	0.97
		90	2.3	1.8	-8.3	72.4	1.2	4.2	-4.4	6.1	1.01	0.71	1.00

Note: $(x/d_{cf})_{\text{theory}} = (\text{conversion factor}) \times (x/d_{cf})_{\text{code}}$

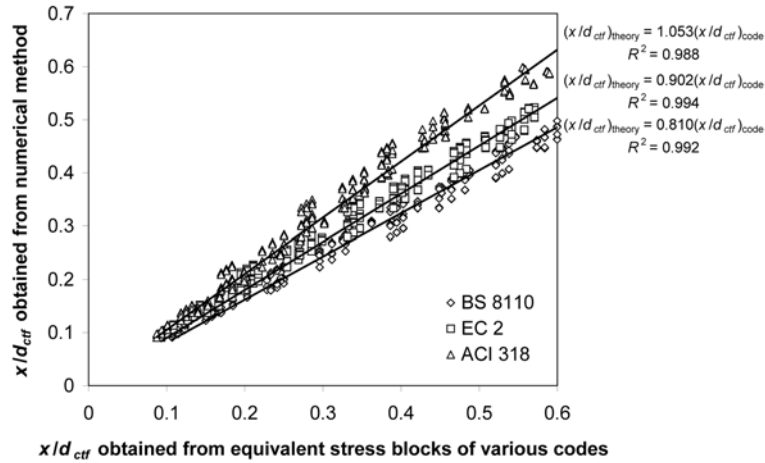


Fig. 16 Relationship between x/d_{crf} ratios obtained from numerical method and various design codes for beams with $f_{co} = 30$ MPa, $d_p = 0.85h$ and $f_y = 460$ MPa

ε_t can be estimated as

$$\varepsilon_t = \frac{0.003(1-x/d_{crf})}{x/d_{crf}} \quad (10)$$

Therefore, Eq. (9) may also be applied to ACI318.

Eq. (9) is based on the concrete model of Attard and Setunge (1996) with a shape different from those in design codes BS8110, EC2 and ACI318. The methods to predict the tendon stress at ultimate and the x/d_{crf} ratios are also different. Moreover, partial safety factors for material are incorporated in the equivalent stress blocks of BS8110 and EC2 which are not taken into account in the numerical analysis. To correct for the discrepancies among the x/d_{crf} ratios obtained from design codes and numerical analysis, a conversion factor is introduced to convert the x/d_{crf} ratios predicted by the codes to that used in Eq. (9). Fig. 16 compares the predictions of x/d_{crf} ratios from numerical analysis with those from design codes for beams having the same depth to prestressing tendon, *in situ* concrete strength and steel yield strength. The strong correlation between various predictions, with all correlation coefficients not less than 0.983, enables conversion factors to be worked out and they are shown in Table 1.

6. Limits for minimum curvature ductility

Existing design codes for RC beams usually impose limits on either x/d or ε_t to ensure that a minimum level of ductility is provided. It is desirable that any new limits proposed for UPC beams should comply with the same ductility requirements prescribed for RC beams. It is also assumed that the *in situ* concrete compressive strength and cylinder strength are 72% and 80% of the cube strength f_{cu} respectively (Ho *et al.* 2002). The relevant provisions in the three design codes are summarised as follows:

- BS8110: Clause 3.4.4.4 specifies the neutral axis depth x not to exceed half of the effective depth d of an RC beams. The code, however, does not specify if the same limit applies to PC beams.
- EC2: Clause 5.6.3(2) limits the neutral axis depth to no more than $0.45d$ for $f_{cu} \leq 60$ MPa and $0.35d$

Table 2 Proposed limits for x/d_{cf} and ε_t for UPC beams

Steel yield strength f_y	d_p/h	<i>In situ</i> concrete strength f_{co}	Limits of x/d_{cf} for		Limits of ε_t for ACI318	
			BS8110	EC2	Tension-controlled	Compression-controlled
250	0.60	30	0.68	0.60	0.00336	0.00108
		50	0.55	0.49	0.00347	0.00078
		70	0.47	0.50	0.00454	0.00113
		90	0.41	0.55	0.00554	0.00158
	0.85	30	0.57	0.49	0.00466	0.00181
		50	0.46	0.41	0.00474	0.00139
		70	0.39	0.42	0.00590	0.00177
		90	0.34	0.46	0.00698	0.00229
	1.1	30	0.42	0.36	0.00728	0.00344
		50	0.33	0.30	0.00742	0.00271
		70	0.29	0.31	0.00892	0.00330
		90	0.26	0.35	0.01032	0.00395
460	0.60	30	0.53	0.47	0.00537	0.00213
		50	0.41	0.37	0.00573	0.00166
		70	0.35	0.37	0.00719	0.00219
		90	0.30	0.40	0.00865	0.00266
	0.85	30	0.44	0.38	0.00689	0.00281
		50	0.35	0.30	0.00735	0.00250
		70	0.29	0.32	0.00881	0.00294
		90	0.25	0.34	0.01047	0.00350
	1.1	30	0.33	0.28	0.01002	0.00468
		50	0.26	0.23	0.01037	0.00403
		70	0.22	0.24	0.01283	0.00487
		90	0.19	0.26	0.01502	0.00556
600	0.60	30	0.46	0.41	0.00659	0.00262
		50	0.36	0.31	0.00725	0.00228
		70	0.30	0.32	0.00921	0.00301
		90	0.26	0.35	0.01064	0.00356
	0.85	30	0.40	0.34	0.00846	0.00376
		50	0.30	0.26	0.00922	0.00326
		70	0.25	0.27	0.01115	0.00383
		90	0.22	0.29	0.01295	0.00455
	1.1	30	0.30	0.25	0.01201	0.00576
		50	0.22	0.19	0.01339	0.00538
		70	0.19	0.20	0.01585	0.00602
		90	0.16	0.22	0.01811	0.00686

for higher grades where d is the effective depth. The same limits apply to both RC and PC beams.

- (c) ACI318: According to Clause 10.3, sections are compression-controlled if the net tensile strain in the extreme tension steel ε_t does not exceed the compression-controlled strain limit when the concrete in compression reaches its assumed strain limit of 0.003. The compression-controlled strain limit is the net tensile strain in the reinforcement at balanced strain conditions. For all prestressed reinforcement, it is permitted to set the compression-controlled strain limit equal to 0.002. Sections are tension-controlled if ε_t is not less than 0.005 when the concrete in compression reaches its assumed strain limit of 0.003. Sections with ε_t between the compression-controlled strain limit and 0.005 constitute a transition region.

Adopting the same numerical model but omitting the prestressing tendon, the limiting curvature ductility factors for RC beams could be obtained by trial or error. Consider a typical RC section with $f_{co} = 30$ MPa (or $f_{cu} = 41.7$ MPa), $f_y = 460$ MPa and non-prestressed tension steel at a depth of $0.85h$. Analysis using the requirements of BS8110 and EC2 give equivalent minimum ductility factors of 3.38 and 3.67 respectively. Similarly ACI318 categorises sections with minimum ductility of 4.13 as tensioned-controlled, while those with ductility below 1.48 as compression-controlled. Based on the limits of curvature ductility, new limits of x/d_{cf} and ε_t for UPC beams can be obtained from Eqs. (8) and (9), and are tabulated in Table 2. The limits of x/d_{cf} in Table 2 ensure UPC beams to be designed with equivalent minimum ductility of BS8110 and EC2, while those of ε_t enable UPC beams to be classified as tension- and compression-controlled having equivalent ductility as those sections with the strain limits defined by ACI318.

Clause 4.3.7.2 of BS8110 defines the effective depth d as the depth to the centroid of prestressed steel area A_p . This definition works well in PC beams with a high PPR as the resultant tensile force is closed to the centroid of A_p . However, for PPC beams, the effect of non-prestressed steel cannot be neglected. Following the provisions in BS8110, x/d tends to be over-estimated when the depth to prestressing tendons well exceeds that to non-prestressed steel and hence the ductility is underestimated, and vice versa. On the other hand, EC2 does not specify whether d refers to the depth to prestressing tendons, non-prestressed steel, or something else. It is suggested that for ductility estimation, the effective depth d should be taken as the depth to centroid of tensile force at ultimate d_{cf} if possible and this applies to RC, PC and PPC members. In the design of concrete beams, it is common to design for flexural strength first and then check for flexural ductility if necessary. After the flexural strength is obtained, stresses in prestressed and non-prestressed steel are available, and hence the depth to neutral axis at ultimate moment x and the depth to centroid of tensile force d_{cf} can also be computed.

7. Effect of compression reinforcement on ductility

In the design of RC beams, one may add compression steel if the beam has insufficient curvature ductility or if the x/d_{cf} ratio exceeds the specified limit. Similarly, addition of compression steel also increases the curvature ductility of UPC beams. The results of typical UPC beams in Fig. 17 show that not only is the ultimate moment capacity increased with increasing amount of compression steel, but there is also a slight drop in yield curvature and a rise in ultimate curvature. As a result, the curvature ductility tends to increase with the area of compression steel A'_s . To investigate the effect of compression steel on the ductility of UPC beams with the same reinforcement indices ω or x/d_{cf} ratios, beams with $f_{co}=50$ MPa, $f_y=460$

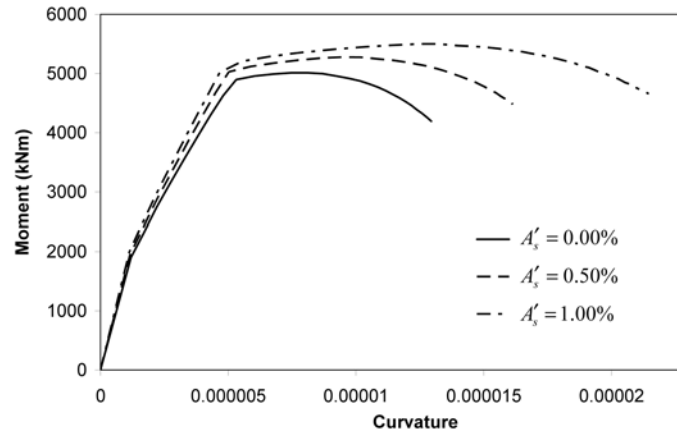


Fig. 17 Full-range behaviour of typical UPC beams with different amounts of compression steel

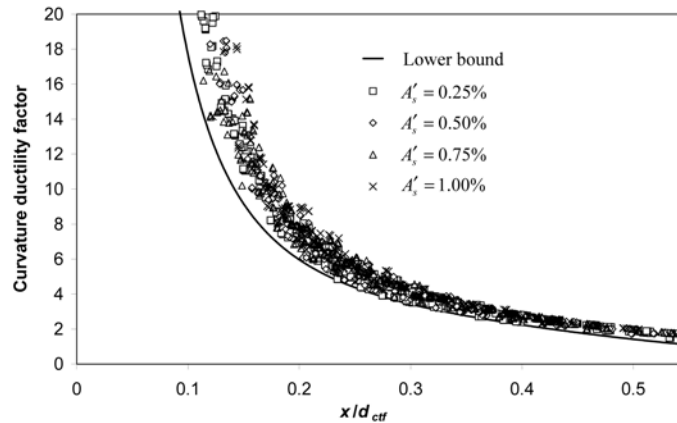


Fig. 18 Relationship between curvature ductility factor μ and x/d_{ctf} for beams of $f_{co}=50$ MPa, $f_y=460$ Pa and $d_p=0.85h$ and provided with compression steel

MPa, $d_p=0.85h$ and $A'_s/bh=0.25\%$, 0.5% , 0.75% and 1% were analysed. The study has examined beams with reinforcement index ω ranging from 0.05 to 0.42 and PPR ranging from 0.04 to 0.89. Fig. 18 shows that the curvature ductility factors of UPC beams with compression steel lie above the lower boundary obtained from parametric studies of beams without compression steel. Therefore Eqs. (8) and (9) provide conservative estimates of ductility of UPC beams with compression reinforcement.

8. Conclusions

The parametric studies carried out on UPC beams indicate that, among various parameters examined, the depth to prestressing tendons, depth to non-prestressed tension steel, partial prestressing ratio, yield strength of non-prestressed tension steel and concrete compressive strength have substantial effects on the curvature ductility. In particular, ductility increases with depth to prestressing tendon, depth

to non-prestressed tension steel and partial prestressing ratio, while it decreases with effective prestress, steel yield strength and concrete compressive strength. At a given tensile force at ultimate ($A_p f_{ps} + A_s f_y$), the ductility increases with concrete compressive strength.

Although the ductility of UPC beams is influenced by many parameters, rather simple equations can be formulated for its evaluation. In view of the different estimates of neutral axis depth ratio x/d_{eff} at ultimate moment by the theory adopted and various design codes, conversion factors have been evaluated so that the equations for estimation of ductility can be used in regular design. Based on the x/d limits in BS8110 and EC2 as well as the ε_r limits in ACI318, new limits are proposed for UPC beams with different concrete compressive strength, yield strength of non-prestressed tension steel and depth to prestressing tendon. The proposed limits ensure that the same level of ductility is provided in UPC beams as in RC beams. The addition of compression steel increases the ductility of UPC beams and therefore the equations developed to predict ductility of UPC beams without compression steel provide safe estimates of ductility.

Acknowledgements

The work described in this paper has been supported by Research Grants Council of the Hong Kong Special Administrative Region, China (RGC Project Nos. HKU 7101/04E and HKU 7102/07E).

References

- ACI Committee 318 (2005), *Building Code Requirements for Reinforced Concrete (ACI 318-05) and Commentary (ACI 318R-05)*, American Concrete Institute, Farmington Hills, MI, USA.
- Allouche, E.N., Campbell, T.L., Green, M.F. and Soudki, K.A. (1998), "Tendon stress in continuous unbonded prestressed concrete members - Part 1: review of literature", *PCI J.*, **43**(6), 86-93.
- Attard, M.M. and Setunge, S. (1996), "The stress-strain relationship of confined and unconfined concrete", *ACI Mater. J.*, **93**(5), 432-442.
- Au, F.T.K. and Du, J.S. (2004), "Partially prestressed concrete", *Prog. Struct. Eng. Mater.*, **6**(2), 127-135.
- Au, F.T.K., Su, R.K.L., Tso, K. and Chan K.H.E. (2008), "Behaviour of partially prestressed concrete beams with external tendons", *Mag. Concrete Res.*, **60**(6), 455-467.
- Bahn, B.T. and Hsu, C.T. (1998), "Stress-strain behavior of concrete under cyclic loading", *ACI Mater. J.*, **95**(2), 178-193.
- British Standards Institution (1997), *BS8110: Part 1: Structural Use of Concrete: Code of Practice for Design and Construction*, BSI, London, UK.
- Du, J.S. and Au, F.T.K. (2009), "Estimation of ultimate stress in external FRP tendons", *Proceedings of the Institution of Civil Engineers-Structures and Buildings*, **162**(4), 213-220.
- Du, J.S., Au, F.T.K., Cheung, Y.K. and Kwan, A.K.H. (2008), "Ductility analysis of prestressed concrete beams with unbounded tendons", *Eng. Struct.*, **30**(1), 13-21.
- Du, G.C. and Tao, X.K. (1985), "Ultimate stress of unbounded tendons in partially prestressed concrete beams", *PCI J.*, **30**(6), 72-91.
- European Committee for Standardisation (2004), *Eurocode 2: Design of concrete structures – Part 1-1: General rules and rules for buildings*, European Committee for Standardisation, Brussels, Belgium.
- Harajli, M.H. (1990), "Effect of span-depth ratio on the ultimate steel stress in unbonded prestressed concrete members", *ACI Struct. J.*, **87**(3), 305-312.
- Harajli, M., Khairallah, N. and Nassif, H. (1999), "Externally prestressed members: evaluation of second-order

- effects”, *J. Struct. Eng-ASCE*, **125**(10), 1151-1161.
- Ho, J.C.M., Kwan, A.K.H. and Pam, H.J. (2002), “Ultimate concrete strain and equivalent rectangular stress block for design of high-strength concrete beams”, *Struct. Eng.*, **80**(16), 26-32.
- Jo, B.W., Tae, G.H. and Kwon, B.Y. (2004), “Ductility evaluation of prestressed concrete beams with CFRP tendons”, *J. Reinf. Plast. Comp.*, **23**(8), 843-859.
- Lin, T.Y. and Burns, N.H. (1981), *Design of Prestressed Concrete Structures*, 3rd Edition, John Wiley & Sons, New York, USA.
- Mattock, A.H. (1967), “Discussion of ‘rotational capacity of concrete beams’ by Corley W”, *J. Struct. Div.* **93**(2), 519-522.
- Menegotto, M. and Pinto, P.E. (1973), “Method of analysis for cyclically loaded R.C. plane frames, including changes in geometry and non-elastic behaviour of elements under combined normal force and bending”, *IABSE Preliminary Report for Symposium on Resistance and Ultimate Deformability of Structures Acted on by Well-Defined Repeated Loads*, 15-22.
- Naaman, A.E. (1985), “Partially prestressed concrete: review and recommendations”, *PCI J.*, **30**(6), 31-71.
- Naaman, A.E. and Alkhairi, F.M. (1991), “Stress at unbonded post-tensioned tendons: Part 1 - evaluation of the state-of-the-art”, *ACI Struct. J.*, **88**(5), 641-651.
- Naaman, A.E., Harajli, M.H. and Wight, J.K. (1986), “Analysis of ductility in partially prestressed concrete flexural members”, *PCI J.*, **31**(3), 64-87.
- Ozkul, O., Nassif, H., Tanchan, P. and Harajli, M. (2008), “Rational approach for predicting stress in beams with unbonded tendons”, *ACI Struct. J.*, **105**(3), 338-347.
- Park, R. and Paulay, T. (1975), *Reinforced Concrete Structures*. John Wiley & Sons, New York, USA.

CC

Notations

A_p	Cross-sectional area of prestressing steel
A_s	Cross-sectional area of non-prestressed tension steel
A'_s	Cross-sectional area of non-prestressed compression steel
b	Width of compression face
d	Effective depth
d_{ctf}	Depth to centroid of tensile force of reinforcement
d_p	Depth to centroid of prestressing tendon
d_s	Depth to centroid of non-prestressed tension steel
d'_s	Depth to centroid of non-prestressed compression steel
E_p	Modulus of elasticity of prestressing steel
E_s	Modulus of elasticity of non-prestressed steel
f'_c	Cylinder strength of concrete
f_{co}	<i>In situ</i> concrete compressive strength
f_{cu}	Cube strength of concrete
f_{pe}	Effective stress in prestressing steel
f_{ps}	Stress of prestressing steel at ultimate
f_{py}	Yield stress of prestressing steel
f_{pu}	Ultimate stress of prestressing steel
f_s	Stress of non-prestressed tension steel at ultimate
f'_s	Stress of non-prestressed compression steel at ultimate
f_y	Yield strength of non-prestressed steel

h	Total height of beam
l	Span length
l_p	Plastic hinge length
q_0	Combined reinforcement index (CRI)
x	Neutral axis depth of beam cross-section
ε_c	Concrete strain
ε_p	Strain of prestressing steel
ε_{pu}	Ultimate strain of prestressing steel
ε_{sp}	Residual plastic strain of steel
ε_t	Net tensile strain in extreme tension steel
ε_{unlo}	Concrete strain on unloading
ϕ_u	Curvature at ultimate
ϕ_y	Curvature at yield
μ_ϕ	Curvature ductility
σ_c	Concrete stress
σ_{ps}	Stress of prestressing steel
σ_s	Stress of non-prestressed steel
σ_{unlo}	Concrete stress on unloading
ω	Reinforcement index